Int J Multiphase Flow Vol 18, No 1, pp. 1–20, 1992
Printed in Great Britain.

0301-9322/92 $5.00 + 0.00

EXPERIMENTAL INVESTIGATION AND PHYSICAL MODELLING OF TWO-PHASE TWO-COMPONENT FLOW IN A CONVERGING–DIVERGING NOZZLE

H. LEMONNIER and S. SELMER-OLSEN†
Commissariat à l'Energie Atomique, Centre d'Etudes Nucléaires de Grenoble, Service de Thermohydrauliques Pour les Applications Industrielles, 38041 Grenoble Cedex, France

(Received 15 May 1990; in revised form 29 July 1991)

Abstract—Two-phase critical flow modelling methodologies are briefly reviewed. When a local knowledge of the flow behaviour is required and the influence of the geometry on the outlet conditions is to be modelled, a two-phase variable slip model is necessary This model requires numerical integration through a singular saddle point. A simple dispersed flow model is presented and integrated numerically. Predictions of this model are compared with data taken on an air–water flow loop capable of producing high gas quality (5–100%) flows of annular dispersed character. It is shown that critical flow solutions of this model have a topological structure qualitatively similar to that of compressible gas flow. However, quantitative deviations are shown, in particular a higher upstream/downstream pressure ratio is necessary to choke the flow. Furthermore, critical flow is experimentally shown to depend on the entrained liquid fraction at the inlet.

Key Words. nozzle, critical flow, two-component, 1-D models, mechanical nonequilibrium, experiments, air–water flow, dispersed annular flow

1. INTRODUCTION

The need for accurate modelling of the dispersion of chemicals released accidentally into the atmosphere has renewed the interest in critical flow phenomena. Two major issues are the critical flow condition (flowrate limitation) and the phase distribution at the point of release. When chemical runaway reaction problems are considered it is generally assumed that a large amount of gas is produced in the vessel and that mass transfer during the discharge can be disregarded. Annular dispersed flow is a probable flow regime for gas qualities in the range between 1 and 100%.

In "classical" critical flowrate models, the interest is mostly limited to global flow parameters like mass flow rates and pressures. When analysed thoroughly, such models appear to be more or less of an empirical nature and place little emphasis on geometrical effects. Moreover, they provide no phase distribution information. A description of the phase distribution at the outlet for annular dispersed flow consists, at the least, of droplet mean diameter and velocity, film thickness and film velocity. It is very unlikely that such quantities are correctly predicted from inlet conditions only, i.e. without accounting for the whole passage through the discharge channel. This can only be done by integrating the set of differential equations modelling the flow, from the given inlet conditions to the outlet of the actual geometry. This could be called an evolution type model. Critical flow conditions will be inherent mathematical properties of this model, related to a singularity in the set of differential equations.

This paper presents parts of an experimental and theoretical study on high-quality critical two-phase flows. In particular, it aims for a better description of the outlet flow characteristics. In section 2, different approaches to critical flow modelling are compared. Next, a 5-equation dispersed flow model is presented. Finally, the two different modelling strategies are discussed in the light of an experimental investigation.

†Permanent address: Det norske Veritas, P.O. Box 300, 1322 Høvik, Norway.

2. MODELLING OF TWO-PHASE TWO-COMPONENT CRITICAL FLOW: STRATEGIES

In this section the two main methods generally utilized for critical flow calculations will be briefly reviewed. A theoretical frame for these calculations was formally established some years ago by Bouré *et al.* (1976). Kestin and collaborators have also over many years worked on topological methods for studying nozzle flows. Recently, Bilicki *et al.* (1987) provided a detailed analysis of the close relationships between the various mathematical singularities of the physical models and the critical flow phenomenon which completes the formal framework for treating critical flows. It will be shown how the same formal methodology leads either to critical flow rate models or to more sophisticated evolution models. Even if the latter are potentially better, the former must not be rejected because they provide easy ways to scale and analyse experimental data. Moreover, provided they are used correctly, they are user-friendly tools for engineering calculations. However, to improve the understanding of critical flow phenomena, evolution modelling seems to be the most rational way from which more simplified global models may benefit at a later stage.

2.1. Methodology

Critical flow phenomena are usually dealt with within the frame of area-averaged (1-D) models. If this restriction is considered, the derivation of a critical flow model consists of four different steps. Global models and evolution models differ only in the last step.

First, a two-phase flow model must be carefully selected. The choice is large and the models may range from the simplest homogeneous model (quasi single-phase flow) to a sophisticated multifield model. The balance equations must be supplemented by the necessary closure relationships in order to produce a consistent model.

Second, the dependent variables of the problem must be chosen. Normally a set of first-order ordinary differential equations (ODEs) results. Most of the time it is a quasi-linear system that reads:

$$\mathbf{A}\frac{\mathrm{d}\mathbf{X}}{\mathrm{d}z} = \mathbf{B}; \qquad [1]$$

$\mathbf{X}$ is the vector formed by the dependent variables, $\mathbf{A}$ is a linear operator that may be a function of $\mathbf{X}$, $\mathbf{B}$ is a vector function depending on $\mathbf{X}$ and z, and z is the abscissa along the flow direction. By solving [1] for the derivatives, two equivalent forms are obtained:

$$\frac{\mathrm{d}X_i}{\mathrm{d}z} = \frac{\Delta_i}{\Delta} \qquad [2]$$

or

$$\left.\begin{aligned} \frac{\mathrm{d}X_i}{\mathrm{d}\zeta} &= \Delta_i \\ \mathrm{d}z &= \Delta\,\mathrm{d}\zeta \end{aligned}\right\} \Leftrightarrow \frac{\mathrm{d}\mathbf{Y}}{\mathrm{d}\zeta} = \mathbf{C}. \qquad [3]$$

Here Δ is the determinant of $\mathbf{A}$, Δ_i is the determinant of the matrix obtained by replacing the ith column of $\mathbf{A}$ by $\mathbf{B}$, ζ is a dummy parameter, $\mathbf{Y}$ is the vector obtained by adding one component (z) to $\mathbf{X}$ and $\mathbf{C}$ is the vector formed by all the determinants.

Third, in order to be critical the solution of the flow model, in a duct with variable cross-sectional area, must cross a singular point of [3]. This condition is fulfilled at the location where the main determinant and one of the secondary determinants are zero:

$$\Delta(\mathbf{X}^*) = 0 \qquad [4a]$$

and

$$\Delta_i(\mathbf{X}^*, z^*) = 0, \qquad [4b]$$

where an asterisk refers to the so-called critical section and Δ_i is one of the determinants in [3]. Moreover, at the singular point $\mathbf{Y}^*$, the linearized version of [3] must have two real eigenvalues of opposite sign. This is a singularity classified as a saddle point.

In the case of a straight or converging pipe, choking may occur if the solution has a turning point at the end of the channel. In this case, it is only accounted for by [4a] and the critical section is the outlet section. A detailed discussion of these aspects is provided by Bilicki *et al.* (1987).

Finally, [4a, b] must be expressed in terms of the control parameters of the process, such as the upstream pressure, the gas and liquid flowrates etc. At this point, two paths are possible:

- Relate the critical parameters to the upstream conditions by *a priori* specifying the nature of the flow evolution (e.g. isothermal, isentropic gas expansion etc.). This leads to global models, the classical analysis where the location of the critical section is assumed rather than derived from [4a, b].
- Relate the critical parameters to the upstream conditions by solving [1] with postulated transfer and closure laws. This yields evolution models.

Whatever the adopted solution is, [4a, b] result in only one equation relating the variables at the inlet of the system. For example, in single-phase flow [4a] means that the velocity of the fluid is equal to the local velocity of sound at the critical section and [4b] tells us where this section is located. If a 2-fluid 6-equation model is considered, the critical flow relationship reads formally:

$$f(\varepsilon, v_G, v_L, p, h_G, h_L)_{inlet} = 0, \qquad [5]$$

where ε is the gas void fraction, v is the velocity, p is the pressure and h is the enthalpy, and where G refers to the gas phase and L to the liquid phase. By recombining the variables a new relationship is obtained:

$$g(M_G, M_L, p, T_G, T_L, \varepsilon)_{inlet} = 0, \qquad [6]$$

where M is the mass flowrate and T is the temperature. It must be noted that f and g account for all the source terms associated with [1] (i.e. heat flux at the walls, wall friction, the geometry and fluid properties).

A correct understanding of [6] is of importance since it provides the list of control parameters of an experimental investigation. In single-phase (gas) flow [6] indicates that the critical mass flowrate is given when the upstream pressure and temperature are given; whereas in two-phase flow it shows that the gas flowrate is imposed when the liquid flowrate, upstream pressure and temperature and the liquid distribution are known. This last statement implies that the gas flowrate may depend on the phase distribution at the inlet even if all the other parameters remain unchanged. This will be shown in section 5.

2.2. Global models ("classical analysis")

This section is not aimed at reviewing critical flowrate correlations. Comprehensive reviews of this topic have already been published (e.g. Giot 1981). Nevertheless, a variant of the constant slip model (CSM) proposed by Henry (1981) will be detailed here as an illustration of section 2.1, and because it will be referred to later on. In the CSM, the ratio of the gas to the liquid velocity is assumed to be a constant. The slip ratio is defined by

$$k \triangleq \frac{v_G}{v_L}. \qquad [7]$$

When no phase change during the process is assumed, the mass quality is constant:

$$x \triangleq \frac{M_G}{M_G + M_L}. \qquad [8]$$

Moreover, if it is assumed that heat transfer between the two phases is sufficiently high, no temperature difference between them will exist:

$$T_G = T_L. \qquad [9]$$

It is further assumed that the walls are adiabatic. In this way the 6-equation model, degenerates to a 3-equation model ([8] replaces one mass balance, [7] replaces one momentum balance and [9]

one total energy balance). By writing the remaining balance equations and keeping only the gas velocity, density and pressure as dependent variables, the following set of ODEs is obtained:

$$\begin{bmatrix} \dfrac{xv_G^2}{(1-x)kv_L + xv_G} & \dfrac{1}{v_G} & 0 \\ 0 & \dfrac{1+x(k-1)v_G}{(1-x)k^2v_G + xkv_L} & 1 \\ -\dfrac{\tilde{C}\tilde{\rho}}{\tilde{C}\tilde{\rho} - R\rho_G}\dfrac{1}{\rho_G} & 0 & \dfrac{1}{p} \end{bmatrix} \begin{bmatrix} \dfrac{d\rho_G}{dz} \\ \dfrac{dv_G}{dz} \\ \dfrac{dp}{dz} \end{bmatrix} = \begin{bmatrix} -\dfrac{1}{A}\dfrac{dA}{dz} \\ -\tau_w \dfrac{\mathscr{P}}{A} \\ \dfrac{\mathscr{P}}{A}\dfrac{\tau_w}{(\tilde{C}\tilde{\rho} - R\rho_G)T} \end{bmatrix}. \quad [10]$$

Here ρ is the density, v is the specific volume, A is the cross-sectional area of the channel, $\mathscr{P}$ is the pipe perimeter, τ_w is the wall shear stress. From the third row of [10] a process similar to a polytropic expansion can be recognized. By assuming $\rho_G \ll \rho_L$:

$$n_e = \frac{\tilde{C}\tilde{\rho}}{\tilde{C}\tilde{\rho} - R\rho_G}, \quad [11]$$

where

$$\tilde{C} = [xC_p + (1-x)C],$$

$$\frac{1}{\tilde{\rho}} = [xv_G + (1-x)kv_L]\frac{(1-x) + xk^2}{(1-x)k + xk^2},$$

C_p is the specific heat capacity of the gas at constant pressure and C is the specific liquid heat capacity. These expressions are close to those of Henry (1981). They are identical when the quality is close to 1, the slip is moderate and $\rho_G \ll \rho_L$.

If the main determinant is set equal to zero, [4a], we obtain at the critical section:

$$G_c^2 = \frac{n_e pk}{[1 + x(k-1)]xv_G}, \quad [12]$$

where G is the mass flux (total mass flowrate divided by the area). For straight and converging channels, [12] applies at the outlet. On the basis of single-phase flow it is normally assumed that [12] applies at the throat, or slightly after, in a converging diverging duct. However, [4b] used on [10] would give the same result.

In order to obtain a useful critical flow model from [12], it is necessary to express it in terms of known quantities (upstream conditions). Unfortunately, a closed form solution of [10] does not exist. Simplifications are necessary. If the wall friction is assumed negligible, the momentum balance may be integrated. Thus, as Henry, (1981) did, by assuming isentropic adiabatic expansion of the gas, p and v_G may be expressed as functions of the upstream conditions:

$$\eta \triangleq \frac{p}{p_0} = \frac{\dfrac{(1-x)kv_L}{xv_G} + \dfrac{\gamma}{\gamma - 1}\eta^{1/\gamma}}{\dfrac{n_e}{2}\left[\dfrac{(1-x)kv_L}{xv_G} + 1\right]^2 + \dfrac{(1-x)kv_L}{xv_G} + \dfrac{\gamma}{\gamma - 1}} \quad [13]$$

and

$$v_G = \frac{RT_0}{p_0}(\eta)^{-1/\gamma}, \quad [14]$$

where subscript zero denotes the upstream stagnation conditions and γ is the specific heat ratio.

It is worth noting that for gas–liquid systems at low pressure, n_e in [11] is essentially equal to 1 except for high gas qualities. This implies that the flow should tend to follow an isothermal expansion rather than an adiabatic one, and that it is inconsistent to assume adiabatic (isentropic) gas expansion. Henry (1981) is not the only modeller to have done this. This aspect will be emphasized in section 5.1.

Finally [12], [13] and [14] may be written as

$$f_{CSM}(G, x, p_0, T_0, k) = 0. \quad [15]$$

The slip ratio k is unknown. If a value of 1 is assumed, the CSM becomes an homogeneous model (HM). Recommended values of k for high-quality flows may be found ranging from 1 to 30 (see Fauske 1965; Giot 1981, 1986; Chisholm 1983). In the CSM, Henry (1981) assumed $k = 3.2$. Most of the time, k values are obtained by correlating data of limited generality. Consequently, these models must be used for geometries and fluids close to those of the experiments. The inaccuracy of these models when they are used beyond these restrictions, is not known *a priori*.

2.3. Evolution models

The alternative solution consists of relating the critical parameters to the upstream conditions by solving [1]. This method is potentially the most powerful since it can account directly for the actual flow conditions (geometry, fluids). In these models the slip between the phase results from the solution itself.

Evolution models require numerical integration. They also need to deal correctly with the mathematical singularity of the set of ODEs. All this work may be handled with low-cost personal computers. Two contributions deserve attention:

- Vromman (1988) calculated critical flows in the homogenizer of a two-phase pump. The model is valid at low gas quality, and this author assumed bubbly flow. Critical flow conditions as well as pressure profiles compared favourably with the experiments under various conditions: air–water flows at low pressure; fuel–nitrogen flows at intermediate pressures (40 bar); and fuel–methane flows where mass transfer is likely to be significant.
- Bilicki *et al.* (1987, 1988; Bilicki & Kestin 1990) proposed a different treatment of the mathematical singularities and succeeded in calculating flashing flows of water. They also described the impact of different closure laws on critical flow. The implementation of this method has not yet been reported for models yielding more than 4 equations. In section 3 Vromman's algorithm will be used with a dispersed flow model of 5 equations.

3. DISPERSED FLOW MODEL

The reason for using a dispersed flow model is to generate slip between the phases by the action of the actual flow conditions and the phases themselves rather than by relying on an external correlation. A simple dispersed thermal equilibrium model is presented. This is considered as a first step towards a future annular dispersed evolution model.

In order to handle correctly the mathematical singularity, brief comments will be given on the solution topology close to the critical section. Finally, by using this information we will solve the model by an iterative forward integration procedure (Vromman 1988).

3.1. Physical model

In this section, the balance equations and the closure laws of the model are presented. It is assumed that neither phase change, nor wall heat transfer occur and heat thermal equilibrium exists between the phases (intensive heat transfer between the phases). Other assumptions are common to all standard 1-D models.

According to this, the model is based on 5 balance equations ($T_G = T_L$ replaces one energy balance). The two mass balances read

$$\frac{d}{dz}(A\varepsilon\rho_G v_G) = 0 \qquad [16]$$

and

$$\frac{d}{dz}[A(1-\varepsilon)\rho_L v_L] = 0. \qquad [17]$$

The momentum balance of the mixture reads

$$\frac{\mathrm{d}}{\mathrm{d}z}\left[A\varepsilon\rho_{\mathrm{G}}v_{\mathrm{G}}^2 + A(1-\varepsilon)\rho_{\mathrm{L}}v_{\mathrm{L}}^2\right] = -A\frac{\mathrm{d}p}{\mathrm{d}z} - \tau_{\mathrm{w}}\mathscr{P}. \qquad [18]$$

The total energy balance of the mixture is given by

$$\frac{\mathrm{d}}{\mathrm{d}z}\left[A\varepsilon\rho_{\mathrm{G}}v_{\mathrm{G}}\left(h_{\mathrm{G}} + \frac{v_{\mathrm{G}}^2}{2}\right) + A(1-\varepsilon)\rho_{\mathrm{L}}v_{\mathrm{L}}\left(h_{\mathrm{L}} + \frac{v_{\mathrm{L}}^2}{2}\right)\right] = 0. \qquad [19]$$

In dispersed flow the liquid is supposed to be present as small droplets. If it is assumed that all the droplets in a cross-section have the same diameter, the momentum balance on a droplet reads

$$\rho_{\mathrm{L}}v_{\mathrm{L}}\frac{\mathrm{d}v_{\mathrm{L}}}{\mathrm{d}z} = -\frac{3}{8}\frac{C_{\mathrm{D}}}{R_{\mathrm{d}}}\rho_{\mathrm{G}}(v_{\mathrm{L}} - v_{\mathrm{G}})|v_{\mathrm{L}} - v_{\mathrm{G}}| - \frac{\mathrm{d}p}{\mathrm{d}z}, \qquad [20]$$

where R_{d} is the droplet radius and C_{D} is the drag coefficient.

At this point the model needs closure laws for the wall friction, the droplet drag coefficient and the droplet radius. As this model is considered as an initial step, the work by Vromman (1988) was followed closely. The drag coefficient is given by

$$C_{\mathrm{D}} = 6.3\,\mathrm{Re}_{\mathrm{d}}^{-0.385}, \quad 10 < \mathrm{Re}_{\mathrm{d}} < 1200. \qquad [21]$$

The droplet Reynolds number (Re_{d}) is based on the physical properties of the continuous gas phase and the slip between the phases. This number is defined by

$$\mathrm{Re}_{\mathrm{d}} \triangleq \frac{2\rho_{\mathrm{G}}|v_{\mathrm{G}} - v_{\mathrm{L}}|R_{\mathrm{d}}}{\mu_{\mathrm{G}}}, \qquad [22]$$

where μ_{G} is the gas absolute viscosity. Vromman (1988) treated bubbly flow and used the analysis of Berne (1983) to close for the bubble radius. Berne (1983) also reviewed models for droplet sizes. He proposed that the maximum droplet size is limited by a turbulent break-up process. The droplet size is controlled by a critical Weber number obtained theoretically. The Weber number is evaluated by using a typical turbulent velocity scale (friction velocity). The friction velocity is defined by analogy with single-phase flow:

$$v_*^2 \triangleq \frac{f}{2}v^2 = \frac{\tau_{\mathrm{w}}}{\rho}, \qquad [23]$$

where ρ and v are the mixture density and velocity, and f is a friction factor;

$$\rho \triangleq \varepsilon\rho_{\mathrm{G}} + (1-\varepsilon)\rho_{\mathrm{L}} \qquad [24]$$

and

$$\rho v \triangleq \varepsilon\rho_{\mathrm{G}}v_{\mathrm{G}} + (1-\varepsilon)\rho_{\mathrm{L}}v_{\mathrm{L}}. \qquad [25]$$

The friction factor is calculated from the pipe Reynolds number of the continuous phase with the Blasius correlation for smooth pipes:

$$f = 0.0791\,\mathrm{Re}_{\mathrm{c}}^{-0.25} \qquad [26]$$

and

$$\mathrm{Re}_{\mathrm{c}} \triangleq \frac{\rho_{\mathrm{G}}v_{\mathrm{G}}D_{\mathrm{c}}}{\mu_{\mathrm{G}}} \qquad [27]$$

where D_{c} is the pipe diameter. Finally, by following Berne (1983), the drop radius is given by the dimensional equation:

$$R_{\mathrm{d}} = \tfrac{1}{2}\mathrm{C}^{3/5}\left(\frac{\sigma}{\rho_{\mathrm{G}}}\right)^{3/5}\left(\frac{\kappa R_{\mathrm{C}}}{v_*^3}\right)^{2/5}\frac{25}{42}, \qquad [28]$$

where R_C is the pipe radius, σ is the gas–liquid surface tension coefficient, κ is the von Karman constant (0.41) and C is a constant given by

$$C = \frac{24}{\pi^2\left(3\frac{\rho_L}{\rho_G} + 2\right)}. \qquad [29]$$

At first sight, it might seem surprising to advocate a droplet size model based on the friction velocity v_* rather than on the slip velocity. However, the model assumes conjoint acceleration of the liquid and the gas from rest up to the throat and not that the liquid is injected at the throat. This latter case would yield a sudden droplet disintegration based on the well-known critical Weber number criterion ($We \simeq 12$).

Kataoka *et al.* (1983) states that there is very strong experimental evidence that drops in steady annular dispersed flow are too small to be generated by sudden exposure to a high velocity gas stream. In other words, a Weber number criterion based on the slip velocity ($v_G - v_L$) would give far too large droplets. The majority of drops are created at the moment of entrainment and the relative velocity between the gas core and the liquid film will determine the droplet size. Kataoka *et al.* (1983) therefore based their droplet size model on the interfacial friction. They could have used the friction velocity equally as well. Moreover, irrespective of the presence of a liquid film, drops or liquid bodies entrained in the core will, due to the turbulent motion, be exposed continuously to the wall shear zone. Berne's (1983) analyses were based on the classical works of Hinze (1955) and Sevik & Park (1973). Considering their description of turbulent emulsification will give a limiting drop size based on the friction velocity. See also, Selmer-Olsen (1991).

By finally considering [16]–[29], a closed-set of 5 ODEs is formed and it must be integrated numerically. Before doing this, some comments must be made on the solution topology.

3.2. Solution topology

Once the form [3] of the balance equations is obtained, a solution curve can be found from a set of initial (upstream) conditions. There are mainly two families of solution curves of physical interest, depending on the choice of initial values. In some cases (as in case A in figure 1) a marching solution curve starts at the inlet and reaches the outlet. The sign of the determinant of the matrix **A**, [1], is the same everywhere. The outlet conditions vary continuously with the inlet conditions: this is subcritical flow. In other cases, the solution curve returns to the inlet (case C in figure 1). This is the so-called "non-physical branch". It represents, in fact, the solution for a nozzle cut exactly at the location of the curve elbow and is a turning point of the solution (e.g. satisfying [4a]). The two families of curves are separated by the $B–B_1$, $B–B_2$ curve. The bifurcation point (*) is a singular critical point of [1] ($\mathbf{C} = 0$ in [3]) and is called a saddle point. Bilicki *et al.* (1987) have shown that the linearized operator describing the solution behaviour at the singular saddle point has 2 non-zero real eigenvalues of negative product and 2 associated eigenvectors, whatever the order of the matrix **A**. The solution bifurcates, as shown in figure 1, in directions given by the components of the eigenvectors and consequently the slopes are finite at the singular point. The

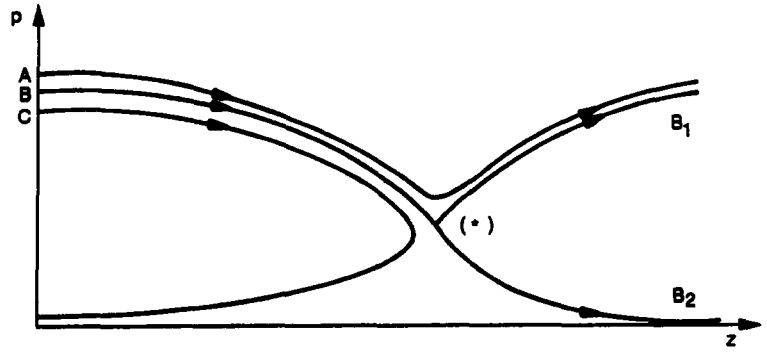

Figure 1. Typical pressure profiles in a converging–diverging nozzle: *, the critical section; A, subsonic curve; C, non-physical branch; $B–B_1$, critical subsonic branch; $B–B_2$, critical supersonic branch

saddle-point topology is a sufficient condition for choking, however singular points other than saddle points may be encountered, as discussed by Bilicki *et al.* (1987).

An important aspect of this solution topology is that it does not contain any description of the shock. In addition to the mathematical reasons emphasized in Bilicki *et al.* (1987) (the number of boundary conditions must match the order of the system), there are some physical reasons. The main physical reason is that the physics of the shock is not contained in [1]. In single-phase compressible flow, the existence of strong normal shocks results from longitudinal heat conduction and from axial normal viscous stresses (Whitham 1971). In the absence of diffusion in our model, only two continuous relaxation free paths are possible downstream of a critical section, and there is no way to recover the outlet pressure without further modelling assumptions. However, many authors when solving the time-dependent counterpart of [1], either deliberately add (for the sake of numerical stability) or have implictly (due to the truncation order of the numerical scheme) diffusion in their models (Roache 1976). This effect is welcome in single-phase compressible gas flow where it allows the pressure profiles to be relaxed towards the back pressure. However, it is more rational to model these effects explicitly.

Here, the key feature is to recognize the singular nature of the phenomenon. Relaxation has a mathematical nature similar to that of a boundary layer. Outside the relaxation zone, the flow is described by [1] (external solution), whereas inside the relaxed zone (inner solution) the different physical processes involved need to be modelled by adding new dependent variables or by including higher order derivative terms with the existing dependent variables. In gas dynamics, the matching of the two models is possible and yields the Rankine–Hugoniot conditions (Whitham 1971). However, in two-phase flow where the mechanisms of relaxation are not completely understood, a reasonable approach consists of carrying out thorough investigations of the solutions of [1]. This establishes the necessary basis (external solution) from which further modelling development can be undertaken.

Two conclusions may be drawn from the above discussion:

(1) In two-phase flow, strong normal shocks cannot be predicted by simply analysing [1].
(2) When experimental data are analysed, fitting closure laws (as friction) to obtain correct predictions (of pressure, for example) is the wrong procedure: if the flow is critical, the supersonic branch of the solution of [1] ($B–B_2$) does not depend on the back pressure; whereas the experimental pressure profile depends on the outlet conditions in a more or less direct way. This will also be discussed in section 5.

3.3. Solution algorithm

According to the discussion in section 2.1 there are 3 main dependent variables in a critical flow experiment. If it is assumed that the two phases enter a given nozzle with the same temperatures and with a given phase distribution, the gas and liquid flowrates and the upstream pressure remain the only dependent variables. If the flow is critical, only 2 out of the 3 may be chosen arbitrarily, [6]. For the sake of convenience it is assumed in what follows that the flowrates are given and that the upstream pressure is unknown and must be guessed.

The idea developed by Vromman (1988) is to use the topology of the solutions to bracket the unknown upstream condition. If a high value of the upstream pressure is chosen, an A-type subsonic solution (figure 1) will be produced, whereas for a lower value of the pressure a C-type curve may result. By refining successively the estimates of the upstream pressure, it is possible to approach as closely as necessary the $B–B_1$ subsonic branch of the solution.

The major drawback of this algorithm is that it does not provide the B_2 branch. However, a very important piece of information is given: the calculated solution corresponds to the onset of criticality, i.e. the upstream pressure below which the flow is critical for given flowrates. This information is never provided by a global model, where criticality does not result from the model, but is assumed. Experimental examples are given and discussed in section 5.

Finally, it must be emphasized that the procedure proposed by Bilicki *et al.* (1987, 1988; Bilicki & Kestin 1990) is superior to that of Vromman (1988) in that it calculates the slopes of both

branches at the saddle point. However, since using this information with a backward integration procedure is not free of technical difficulties for the 5-equation model presented here, its implementation will be published elsewhere (Lemonnier *et al.* 1991).

4. THE FOSSEGRIMEN EXPERIMENT

The flow loop (FOSSEGRIMEN) was built in order to provide experimental data for critical flow conditions. This is basically an air–water flow system which can be operated with a number of different test sections.

4.1. The flow loop

A brief description of the loop is given in figure 2. Its main characteristics are

Gas: 0–400 kg/h up to 9 bar
Liquid: 0–1000 kg/h up to 15 bar.

The liquid circulates in a closed loop, whereas the gas flows through an open circuit.

For the gas side, air is pumped from the ambient atmosphere to a 1 m^3 tank by a 37 kW screw compressor. The pressure is kept constant by an automatic regulation valve at the tank inlet. The

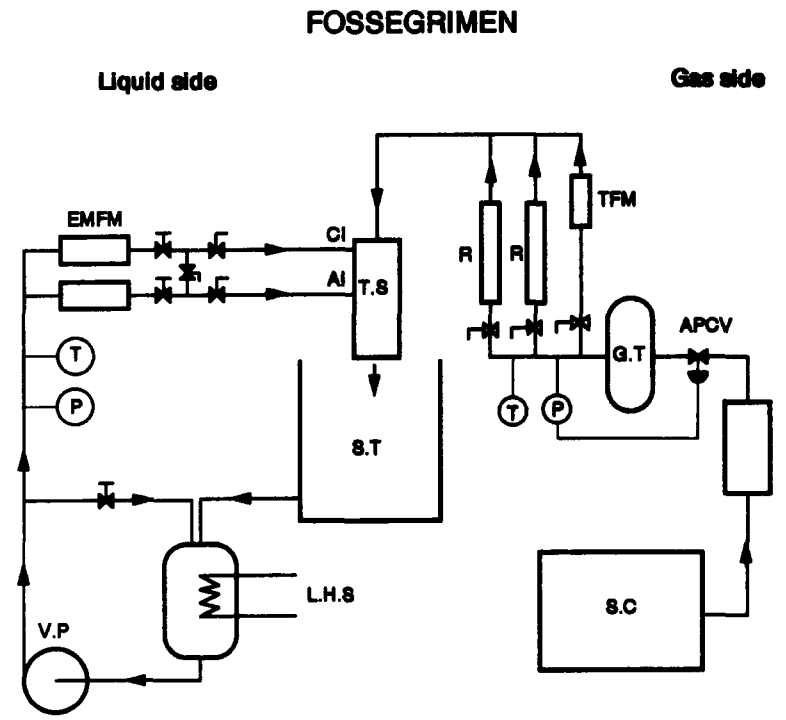

NOMENCLATURE :

APCV : Automatic pressure control valve
ACS : Air conditioning system 20 - 60°C 4.5 kW Dry/oil free filtered air
GT : Gas tank (1m^3)
LR : Liquid reservoir with heating (20 - 60°C) 0.6 m^3 30 kW
EMFM : Electromagnetic flowmeters 0 - .10, 0 -1.0 m^3/h
P : Pressure gauge
R : Rotameter (gas) 0 - 3.5 Nm^3/h 0 - 20 Nm^3/h
SC : Screw compressor 37 kw 0 - 400 Nm^3/h, 0 - 10 bar
ST : Separation tank
T : Temperature gauge
TFM : Turbine flow meter 0 - 65 m^3/h
TS : Test section (vertical downwards flow)
VP : Volumetric pump 0 - 40 bar at 1 m^3/h
CI : Central injection of liquid
AI : Annular injection of liquid

Figure 2. The Fossegrimen loop.

test section is fed from this tank and air is metered either through a 65 m^3/h turbine flowmeter or smaller range rotameters.

For the liquid side, water is pumped from a collection tank by a volumetric pump. Flow rate regulation is achieved by by-passing part of the flow back to the pump. Liquid is metered by electromagnetic flowmeters and injected in a mixing section upstream of the nozzle.

At the outlet of the test section a silencer is installed in order to reduce the noise level. Here the liquid and the gas are separated: air is released to the atmosphere and liquid returns back to the collection tank.

The control parameters of the loop are:

- The upstream pressure.
- The liquid flowrate.
- The entrance conditions (liquid and gas repartition).
- The temperature of the two fluids.
- The test section geometry.

4.2. The test section

The test section is an axisymmetric converging–diverging nozzle with 5 mm throat diameter. The transition from conical to cylindrical sections is graduated over a short channel length having a circular arc with high curvature. This nozzle is shown in figure 3. It is made of clear plexiglass to allow direct visualization of the flow. The liquid may be injected either centrally or at the vicinity of the wall as a thin liquid film. This design allows us to study the effects on the critical flowrate of the liquid distribution at the inlet of the nozzle. Detailed views of the injection sections are shown in figure 4.

5. EXPERIMENTAL RESULTS AND DISCUSSION

Experimental results obtained in the 5 mm nozzle are presented here. Next, the effect of upstream pressure and the inlet geometry on the mass flowrate is discussed. Finally, typical experimental pressure evolutions are presented and compared with the evolution model.

5.1. Critical flowrate data: upstream pressures and inlet geometry effects

Critical flowrate data obtained with the FOSSEGRIMEN flow loop are shown in figures 5 and 6 where they are compared with the HM and CSM of section 2.2. The liquid injection in these

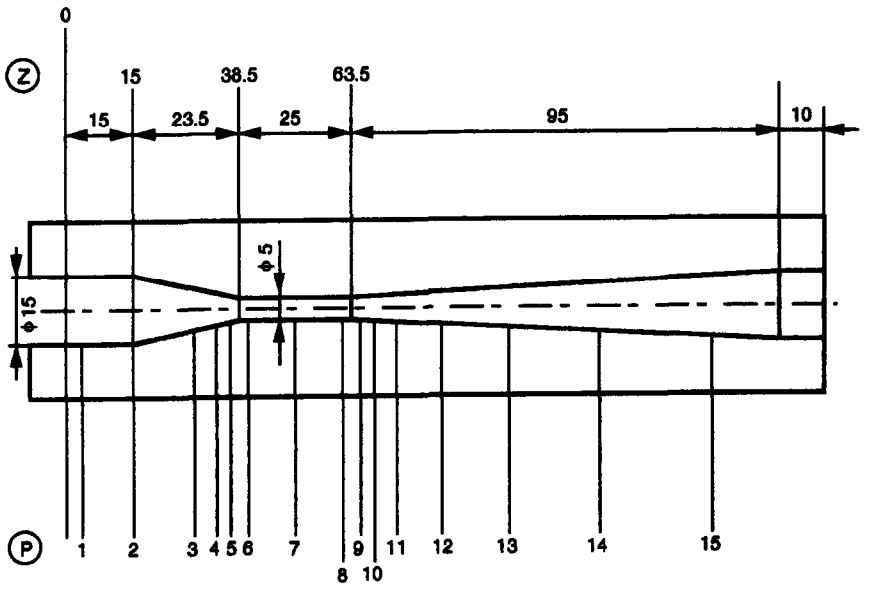

Figure 3. The 5 mm converging–diverging nozzle.

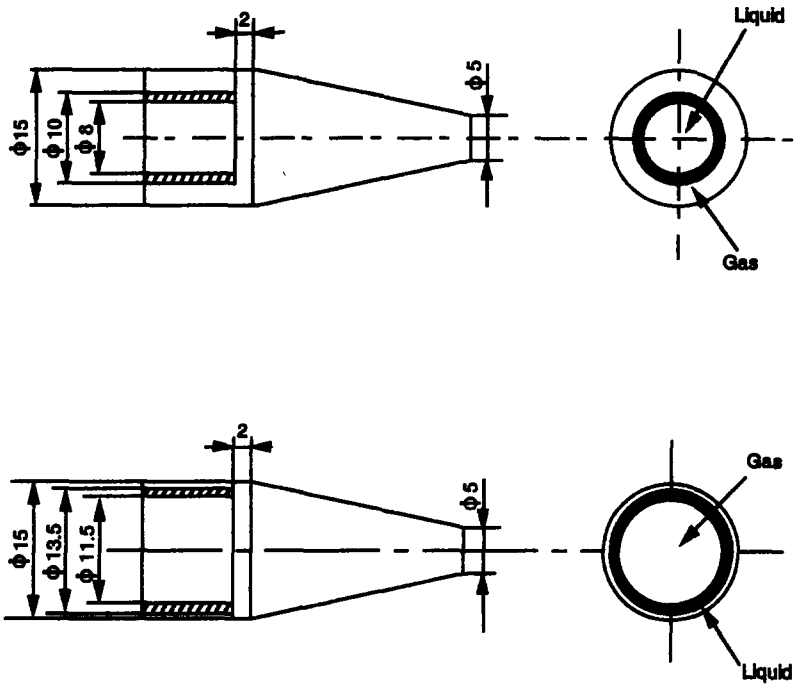

Figure 4. The two liquid injection devices

experiments is central (figure 4). The continuous lines represent the model predictions, whereas the symbols represent data points.

Apparently, both the nozzle geometry and the central injection favour a relatively homogeneous flow behaviour. Furthermore, note that the higher the pressures, the closer the experiments are to the HM. This is an effect of the level of mechanical non-equilibrium. Increasing the pressure, increases the gas density and thus the drag force on the droplets, i.e. resulting in a higher rate of momentum transfer between the gas and liquid phases. The 8 bar data (the highest pressure in the experiments) follow the HM closely, whereas the lower pressure data is well-represented by the CSM with a moderate value ($k = 1.2$) of the slip ratio, as shown in figure 6. Moreover, the slip ratio is seen to be a function of the pressure (gas density), as already mentioned by Fauske (1965) and Chisholm (1983).

The effect of annular liquid injection is shown in figures 7 and 8, where the critical flow data are compared with the HM and the CSM. Figure 7 shows that the mechanical non-equilibrium remains significant even at the highest test pressure (compare also with figure 5): the HM does not fit the data satisfactorily; whereas the CSM with a moderate value of slip ratio ($k = 1.2$ again) represents all the data correctly. It seems that the pressure dependency on the slip ratio vanishes. This may be an indication of a different acceleration process for purely annular flow at the inlet.

The presented data demonstrate that for a given liquid flowrate, upstream pressure and temperature, the gas mass flowrate depends on the fraction of the liquid which is initially entrained in the gas flow. Direct observations and high-speed ciné films show that when the liquid is injected centrally, a liquid jet is formed which immediately breaks up and generates small droplets entrained in the gas stream. This process produces a high specific interfacial area and the acceleration of the liquid is high. On the contrary, when the liquid is injected as a film close to the wall, the entrainment process is totally different. In many cases, the film enters the throat of the nozzle and the mixing of the two phases takes place farther downstream. The acceleration of the liquid is delayed and this gives a higher level of mechanical non-equilibrium. Since a higher gas flowrate is a consequence of a higher mechanical non-equilibrium, the annular injection data suggest the presence of a liquid film containing more mass than when the central injection is used. If the interfacial friction is the only mechanism to reduce the slip velocity between the two phases, it may be assumed

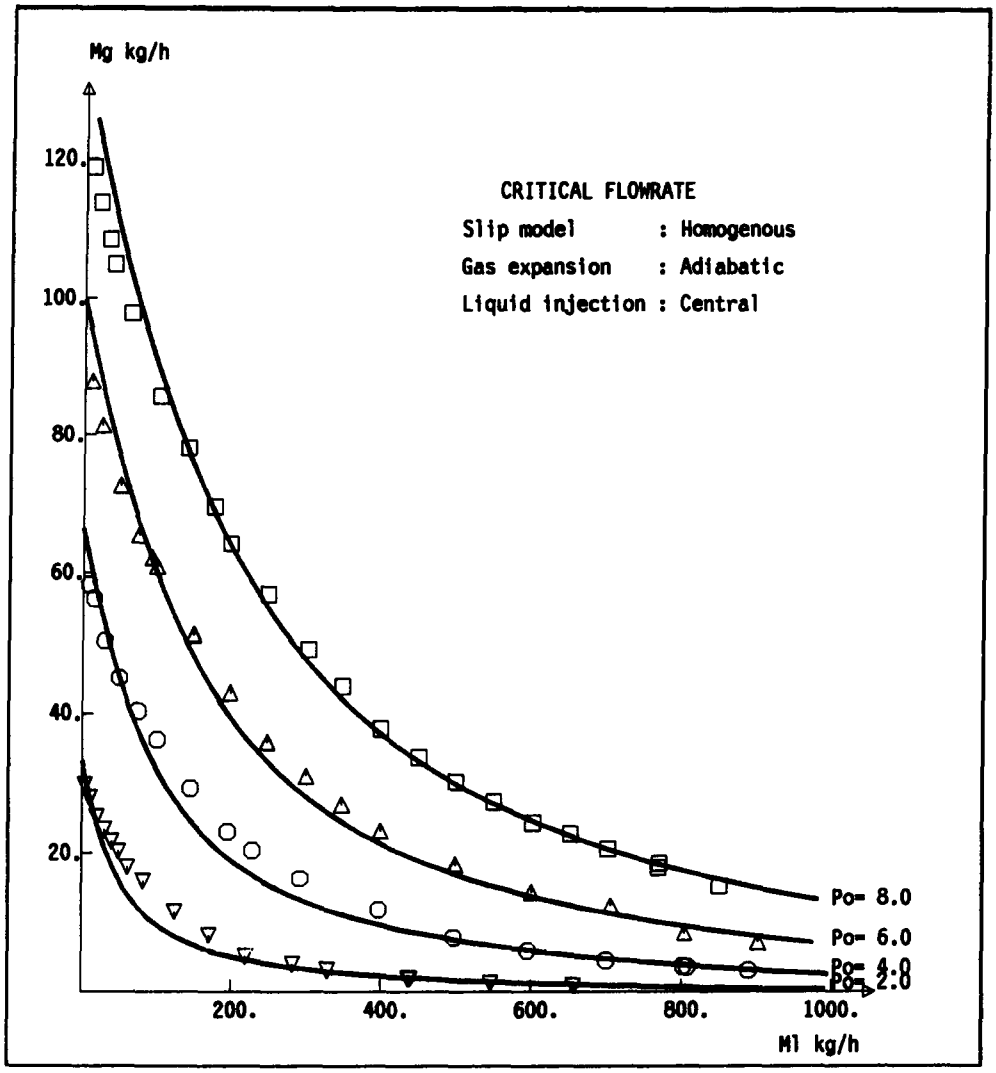

Figure 5. Critical flowrate data. Liquid injected centrally and the HM. Gas flowrate as a function of the liquid flowrate for different values of the pressure: □, 8 bar; △, 6 bar; ○, 4 bar; ▽, 2 bar.

that a shorter throat will show greater differences in the gas flowrate between the two injection modes.

In figure 9 the data are compared with the evolution model (EM) presented in section 3.1. Only the data corresponding to central injection of the liquid are kept for the comparison. The highest flowrate point for each pressure condition is single-phase flow. Significant discrepancies appear for the higher qualities and the highest pressure points (6 and 8 bar) where the HM seemed to represent the data correctly (see figure 5). This apparent paradox can be explained by considering the inconsistency of the HM mentioned in section 2.2. It was indicated in section 2.2 that due to the form of the third equation of [10] the flow was isothermal rather than isentropic. Correct accounting for this (by replacing the unjustified isentropic gas expansion) is possible by simply replacing γ by n_e in [13]. This yields the corrected constant slip model (CCSM) which has the corrected homogeneous model (CHM) as a special case for a slip ratio of 1. Figure 10 shows that the CHM also underpredicts the data in the same qualitative way that the EM does (figure 9). However, the EM is quantitatively better. Moreover, the single-phase gas flow data in figures 10 are overpredicted by the CHM due to its frictionless nature. This comparison of the CHM with data proves that the slip is still significant for the high-pressure data and that the good prediction by the HM in figure 5 was pure chance. Finally, this shows how unwise it could be to rely on a

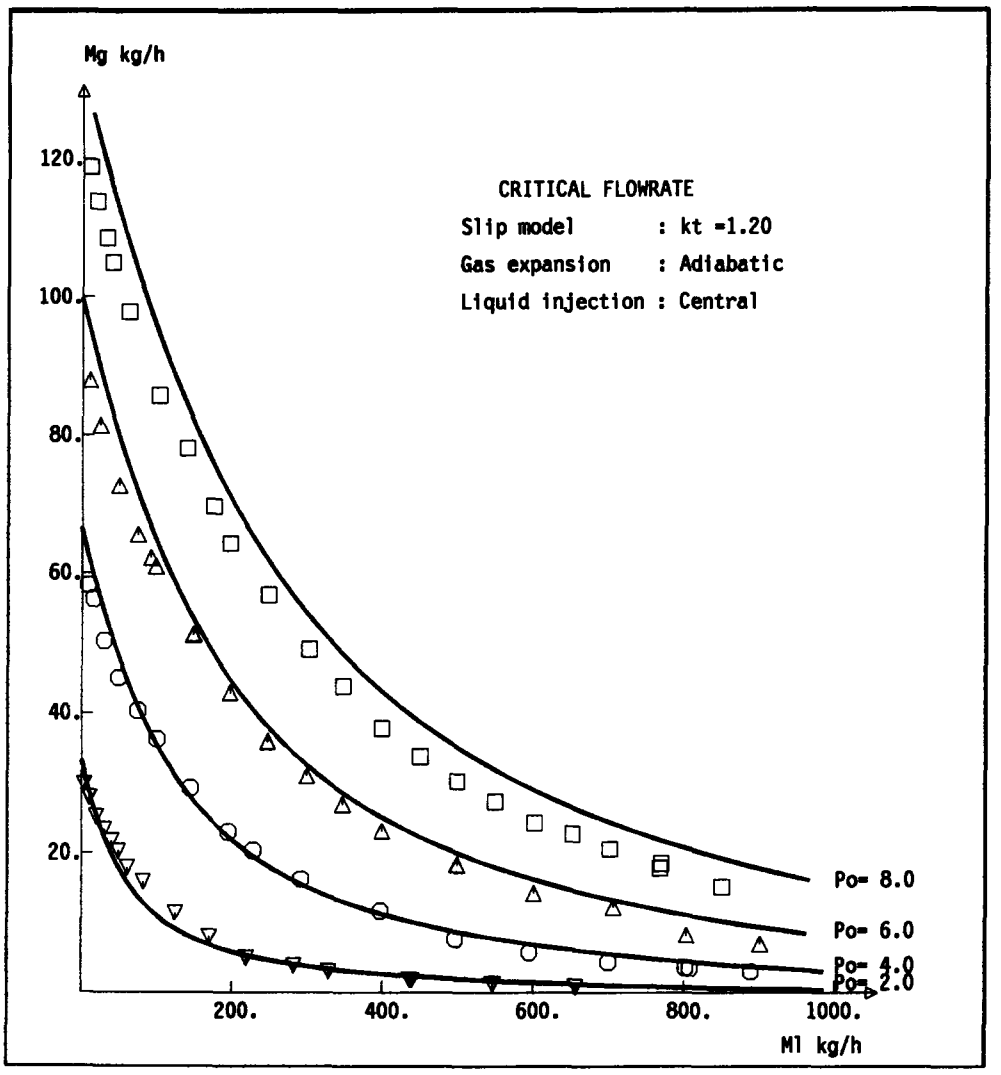

Figure 6. Critical flowrate data. Liquid injected centrally and the CSM. Gas flowrate as a function of the liquid flowrate for different values of the pressure: □, 8 bar; △, 6 bar; ○, 4 bar, ▽, 2 bar.

critical flowrate model with a single adjustable constant: minor inconsistencies may be compensated for by an appropriate experimental fitting, thus hampering the physical meaning of the model.

By comparing figures 9 and 10 it appears that the EM is better at predicting the low-quality data. Sensitivity calculations proved that no admissible changes in the closure laws of the EM (e.g. increased droplet sizes) may reconcile the predictions and data. The conclusion being that an improved model should account for a liquid film to allow more mechanical non-equilibrium. Another indication for this is provided by Azzopardi *et al.* (1989), who showed that for a converging–divering nozzle with a 10 mm throat diameter only 25% of the liquid mass was entrained as droplets. The work of Martindale & Smith (1982) also shows the importance of the liquid film. Consequently, it is envisaged to improve the present EM by adding to it a description of the liquid film.

5.2. Pressure evolutions

Figures 11 and 12 show pressure profiles measured in the nozzle in figure 3, the liquid injection upstream being central. The liquid flowrates are 93 kg/h in figure 11 and 498 kg/h in figure 12,

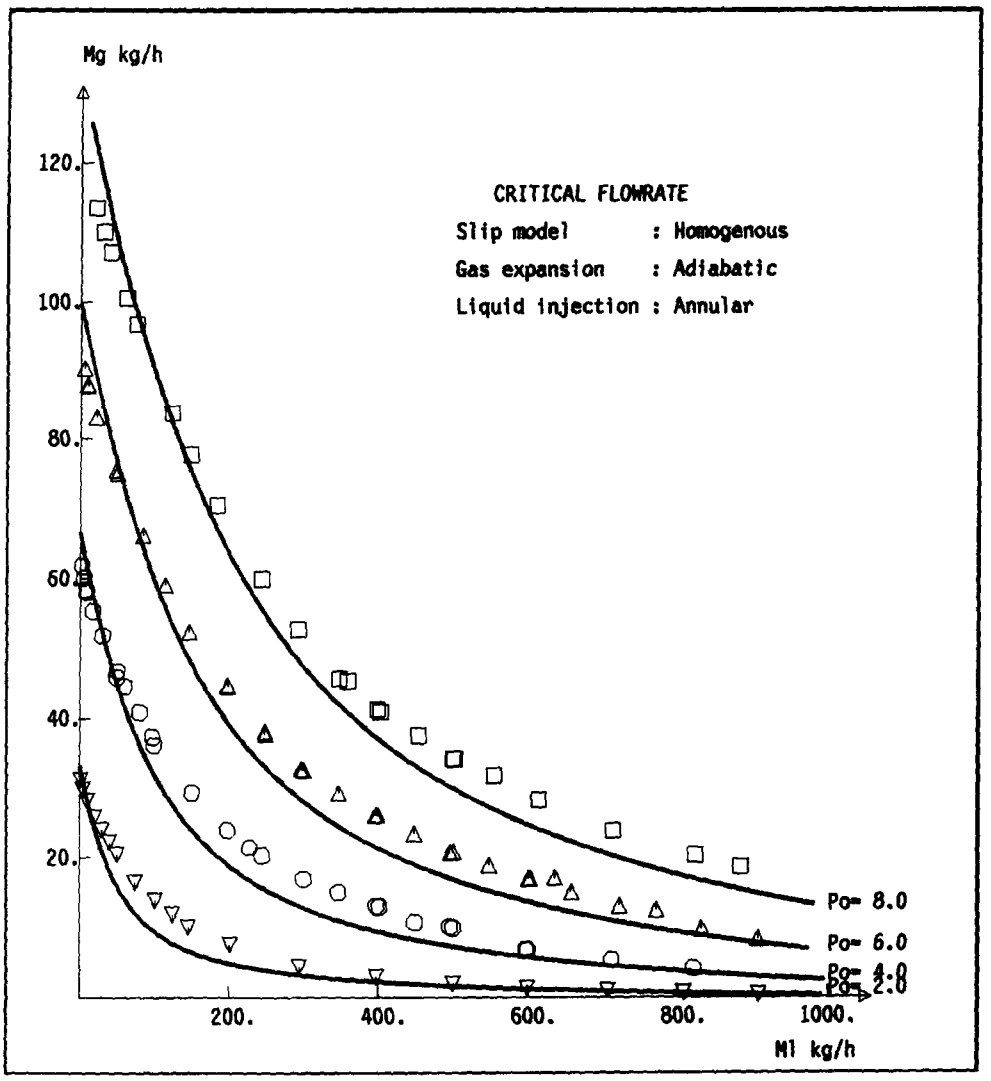

Figure 7 Critical flowrate data Annular liquid injection and the HM. Gas flowrate as a function of the liquid flowrate for different values of the pressure: □, 8 bar; △, 6 bar; ○, 4 bar; ▽, 2 bar.

respectively. The upstream pressure is 6 bar. For constant inlet conditions, the introduction of a flow restriction at the outlet permitted a gradual decrease in back pressure down to atmospheric, a classical way to produce choked/critical flow.

The experimental data points in figure 11 resemble the well-known topological behaviour of single-phase compressible nozzle flow under similar conditions. In particular, for the lowest back pressure values, the pressure profiles seem to gather along a unique curve from which relaxation to the outlet pressure is visible. Moreover, a critical section can be identified just downstream of the throat for which neither upstream data points nor the gas flowrate are affected by a further decrease in the back pressure. It must be noted here that in single-phase flow, due to the sparse distribution of the pressure taps, direct observation of normal shocks close to the throat end was not possible. However, for a further reduction in back pressure, no evidence of sharp recompression was found. It is thought that, in agreement with what is described by Summerfield *et al.* (1954), a compressible flow separation occurs and interferes with the shock formation. The test conditions of figure 11 are given in table 1 along with the calculated gas mass flowrates.

The data points in figure 12 show a profile of another character. Even for the lowest outlet pressure, a critical section cannot be identified easily inside the diverging part of the nozzle. Test

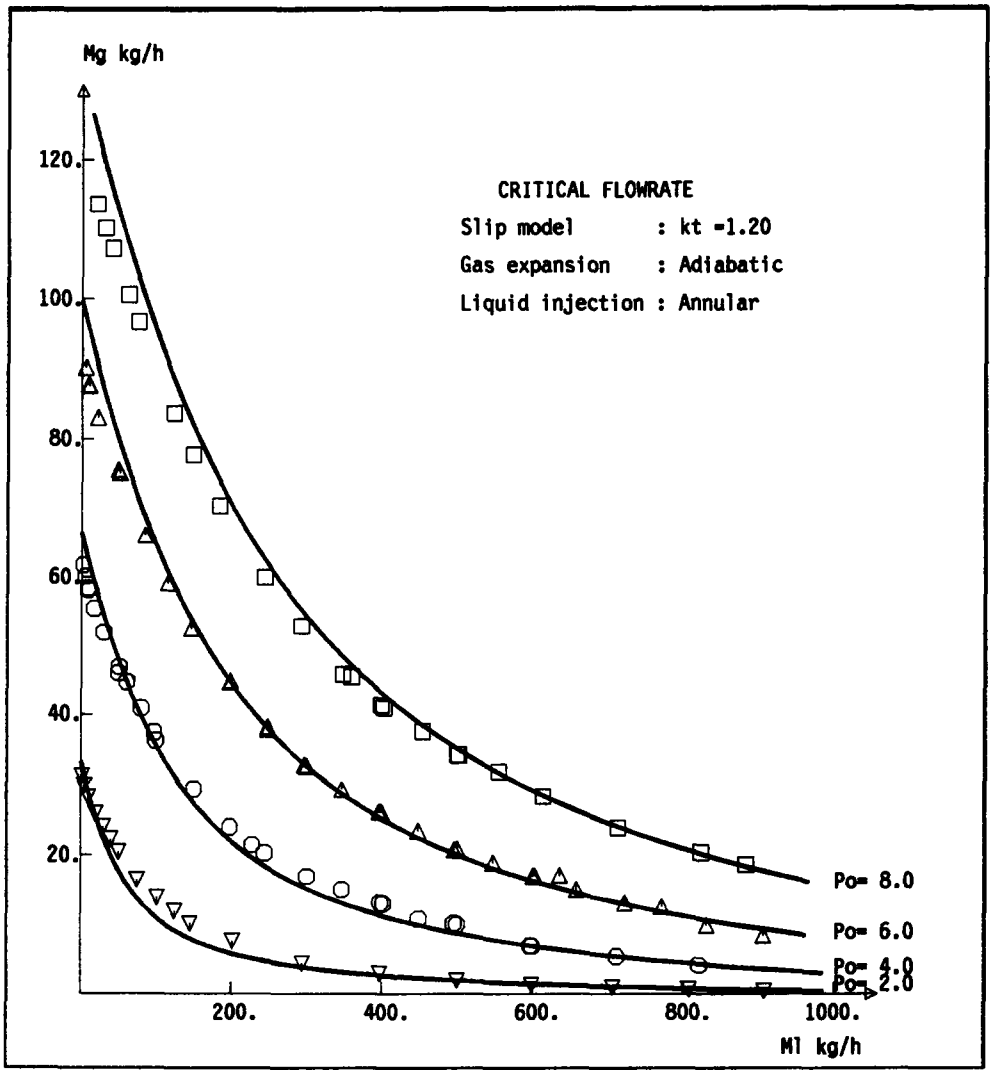

Figure 8. Critical flowrate data. Annular liquid injection and the CSM. Gas flowrate as a function of the liquid flowrate for different values of the pressure: □, 8 bar, △, 6 bar, ○, 4 bar; ▽, 2 bar.

conditions and calculated values of the gas mass flowrate are given in table 2. Even though the pressure profiles do not give any indication of choking, the mass flowrate is barely affected by the decrease in back pressure. However, it must be noted that due to the use of class 4 gas rotameters for the data in figure 12, eventual variations in the corresponding mass flowrate are beyond the measurement accuracy. The general impression from figure 12 is that the topological pattern of the pressure profiles seems to be a subcritical nature.

Table 1

P_{outlet} (bar)	Gas rate (kg/h)	
	Exp.	Calc.
5.38	37.2	32.9
4.64	54.1	49.6
4.30	58.4	52.0
3.80	61.1	52.7
3.10	62.0	52.7
2.00	62.1	52.7
1.28	62.4	52.7
0.81	62.2	52.7

Table 2

P_{outlet} (bar)	Gas rate (kg/h)	
	Exp.	Calc.
5.54	3.2	2.5
4.50	10.0	12.6
3.62	15.4	16.8
2.44	18.2	18.7
1.93	19.1	18.9
1.39	18.5	19.1
0.93	18.4	18.9

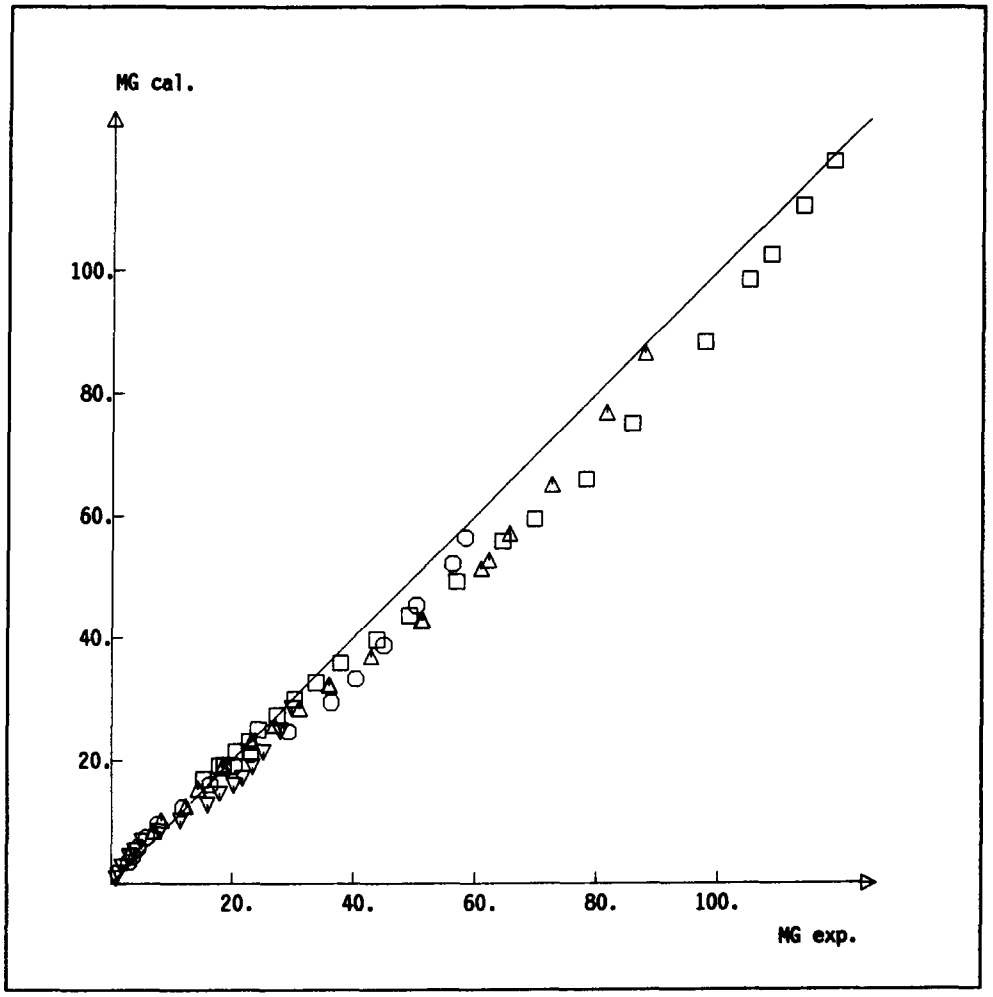

Figure 9. Critical gas flowrate compared with the EM (liquid injected centrally) for different values of the pressure: □, 8 bar; △, 6 bar; ○, 4 bar; ▽, 2 bar.

The continuous profiles in figures 11 and 12 are calculated by the present EM. Where a subcritical solution is possible, for the given experimental upstream pressure and liquid flowrate, the gas mass flowrate is calculated such that the calculated outlet pressure attains the experimental value. Wherever this adjustment is not possible, the critical solution, branch B–B_1 in figure 1, was obtained. The EM reproduces the topological nature of the pressure profiles given in figures 11 and 12. A saddle point is present for the lowest liquid flowrate, whereas subcritical flow is calculated for all conditions of figure 12 except the lowest back-pressure value. In this case, the calculation seems to indicate choking close to the minimum of the pressure profile, i.e. in the middle of the diverging section. These data and calculations could be confirmation that choking can occur anywhere in a diverging channel section, as stated by Bilicki *et al.* (1987; Bilicki & Kestin 1990).

Another characteristic behaviour of 1-D models is found in the proposed EM. This model obviously overpredicts the pressure recovery in the diffuser. This is not seen directly from figure 11 due to the calculation technique which forces the calculated upstream and downstream pressures to coincide with the data. As a result the largest discrepancies appear in the throat area. It is easily imagined that if the pressure was set close to the diffuser inlet, instead of its outlet, the calculated outlet pressure would exceed the measured value.

Next, when the CSM, [10], is integrated numerically, the calculated pressure profiles always resemble single-phase gas profiles. The calculated critical section is close to the throat end, the

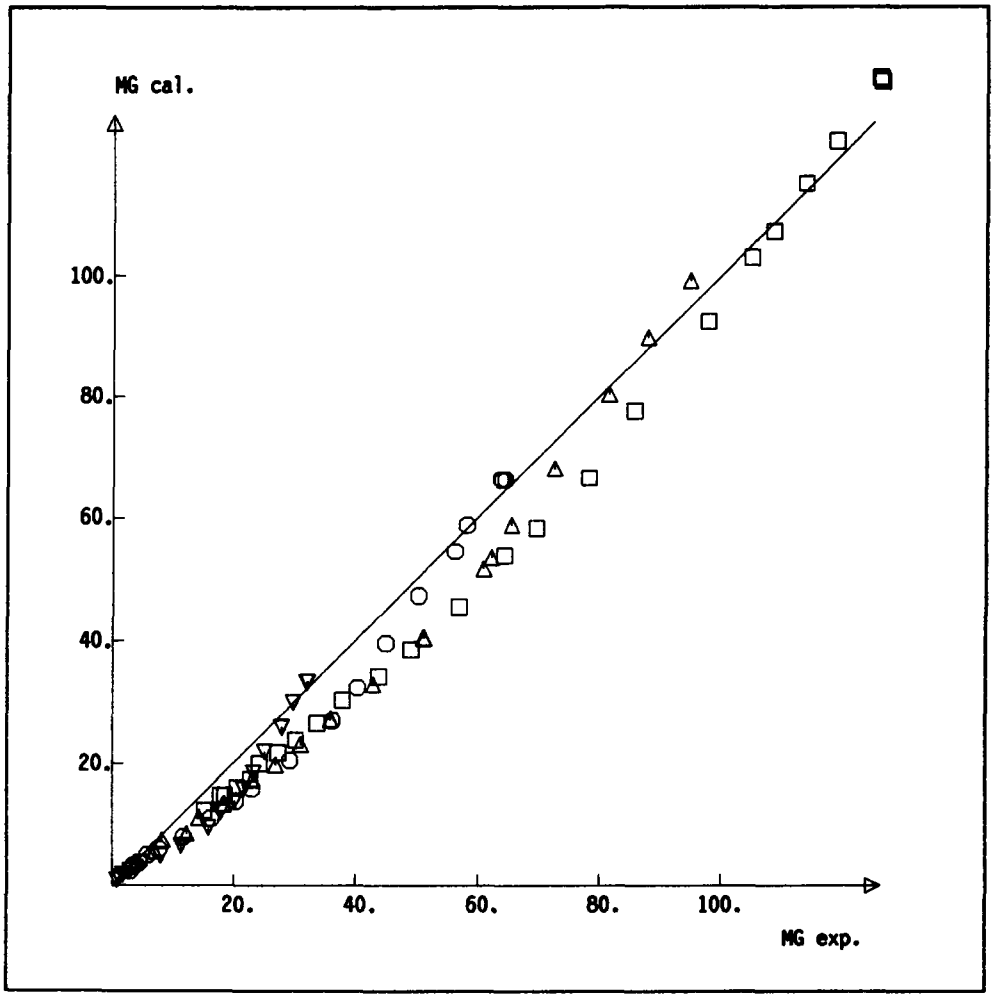

Figure 10. Critical gas flowrate compared with the corrected HM (liquid injected centrally) for different values of the pressure: □, 8 bar; △, 6 bar; ○, 4 bar; ▽, 2 bar.

critical pressure ratio is close to the single-phase value (0.5) and the pressure recovery in the diffuser is almost complete since the only loss in momentum is due to friction. Even if a CSM is able to estimate the correct value of the mass flowrate, it should be noted that it is unable to reproduce the trends discussed above.

6. CONCLUSIONS

It has been shown that "classical" critical flowrate models, though user-friendly tools for engineering calculations, are unable to predict geometrical effects, the effect of the liquid repartition at the inlet and the position of the critical section. In particular, it has been shown that the hypothesis for the location of the critical section is not always justified and that the critical pressure ratio values of the CSM are sometimes inadequate. To overcome these deficiencies a simplified dispersed flow EM has been proposed and integrated numerically.

Experiments have shown that critical flow phenomena depend on the liquid fraction entrained at the inlet. Moreover, it has been shown by progressively decreasing the outlet pressure that low gas quality flow might remain subcritical in nature even if the upstream/downstream pressure ratio is as high as 6 : 1. This last experimental finding, among others, is reproduced by the present EM.

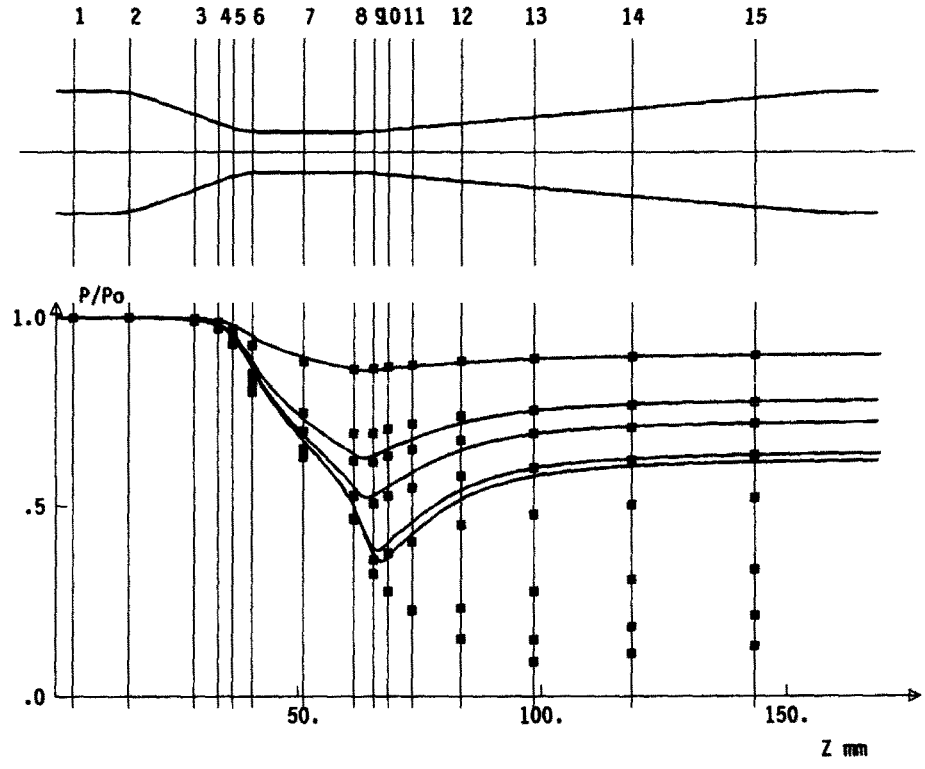

Figure 11. Pressure profiles. Inlet pressure = 6 bar, liquid flowrate = 93 kg/h. For other parameters see table 1.

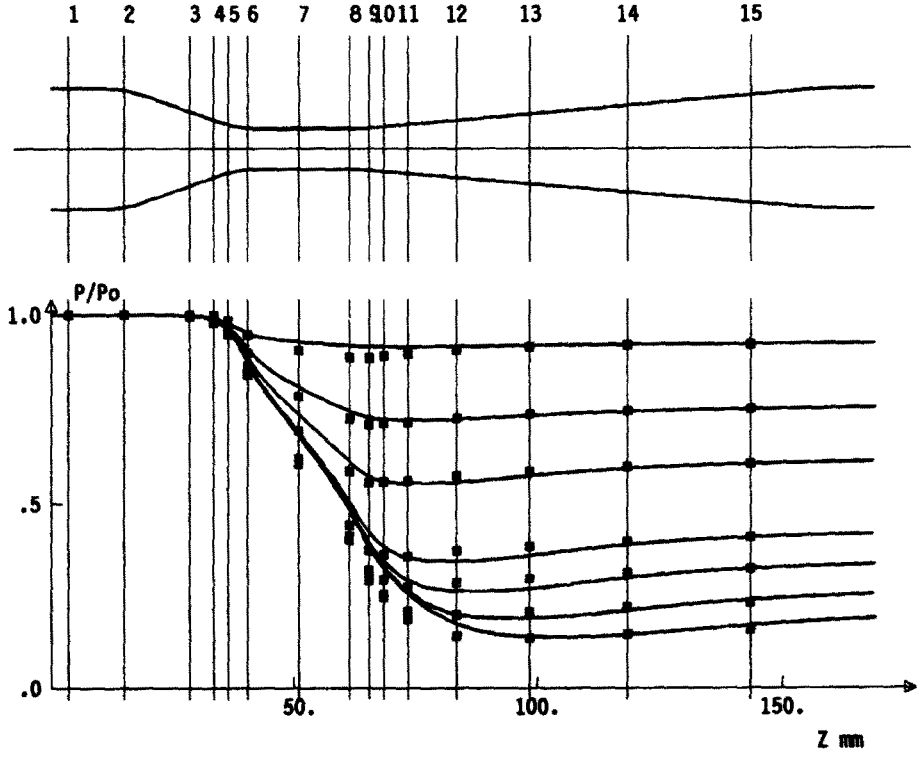

Figure 12. Pressure profiles. Inlet pressure = 6 bar, liquid flowrate = 498 kg/h. For other parameters see table 2.

Finally, analysis of the data by both classical models and the presented EM has suggested that, even if a reasonable level of understanding has now been reached in critical flow modelling strategy, some physical effects are not yet accounted for correctly in the proposed EM:

- A liquid film description ought to be added in future work.
- The 2-D effects (detachment zones) may be modelled advantageously by a technique developed by Azzopardi *et al.* (1988).

However, the modelling of the relaxation of the flow to the outlet conditions, due to its probable singular nature, still remains an open question.

REFERENCES

AZZOPARDI, B. J., TEIXEIRA, S. F. C. F., GOVAN, A. H. & BOTT, T. R. 1988 An improved model for flow in a venturi. UKAEA Report AERE R13060.

AZZOPARDI, B. J., MEMORY, S. B. & SMITH, P. 1989 Experimental study of annular flow in a venturi. In *Multiphase Flow Proc. of the 4th Int. Conf., Nice*, pp. 199–214. BHRA, Cranfield, Beds.

BERNE, PH. 1983 Contribution à la modélisation du taux de production de vapeur par autovaporisation dans les écoulements diphasiques en conduite. Thèse de Docteur Ingénieur, Ecole Centrale des Arts et Manufactures, Paris, France.

BILICKI, Z. & KESTIN, J. 1990 Physical aspects of the relaxation model in two-phase flow. *Proc. R. Soc. Lond.* **428A,** 379–397.

BILICKI, Z., DAFERMOS, C., KESTIN, J., MAJDA, J. & ZENG, D. L. (1987) Trajectories and singular points in steady-state models of two-phase flows. *Int. J. Multiphase Flow* **13,** 511–533.

BILICKI, Z., KESTIN, J. & PRATT, M. M. 1988 The effect of three closures on critical conditions in two-phase flow with unequal phase velocities. *Int. J. Multiphase Flow* **14,** 507–517.

BOURE, J. A., FRITTE, A. A., GIOT, M. M. & REOCREUX, M. L. 1976 Highlights of two-phase critical flow: on the link between maximum flowrates sonic velocities, propagation and transfer phenomena in single and two-phase flows. *Int. J. Multpase Flow* **3,** 1–22.

CHISHOLM, D. 1983 *Two-phase Flow in Pipelines and Heat Exchangers.* George Godwin, London. ISBN 0-7114-5748-4.

FAUSKE, H. K. 1965 Two-phase two- and one-component critical flow. In *Proc. Symp. on Two-phase Flow, Exeter*, Vol. 1 (Edited by LACEY, P. M. C.), pp. 101–114. Dept Chem. Engng, Univ. of Exeter, Devon.

GIOT, M. 1981 Critical flows. In *Thermalhydraulics of Two-phase Systems for Industrial Design and Nuclear Engineering* (Edited by DELHAYE J. M., GIOT, M. & RIETHMuller, M.), pp. 405–452. Hemisphere, Washington, DC.

GIOT, M. 1986 Critical flow. *von Karman Institute for Fluid Dynamics, Lecture Series No. 3,* Rhode-saint-Genèse, Belgium.

HENRY, R. E. 1981 Calculation techniques for two-phase critical flow. In *Two-phase Flow Dynamics, Japan–U.S. Seminar 1979* (Edited by BERGLES, A. E. & ISHIGAI, S.), pp. 415–436. Hemisphere, Washington, DC.

HINZE, J. O. 1955 Fundamentals of the hydrodynamic mechanism of splitting in dispersion processes. *AIChE Jl* **1,** 289–295.

KATAOKA, I., ISHII, M. & MISHIMA, K. 1983 Generation and size distribution of droplet in annular two-phase flow. *Trans. ASME, J. Fluids Engng* **105,** 230–238.

KESTIN, J. & ZAREMBA, S. K. 1953 Geometrical methods in the analysis of ordinary differential equations. *Appl. Scient. Res. Sect. B* **3,** 149–189.

LEMONNIER, H., SELMER-OLSEN, S., AARVIK, A. & FJELD, M. 1991 The effect of relaxed mechanical non-equilibrium on gas–liquid critical flow modeling. Presented at the *27th ANS Natn. Heat Transfer Conf.*, Minneapolis, MN.

MARTINDALE, W. R. & SMITH, R. V. 1982 Separated two-phase flow in a nozzle. *Int. J. Multiphase Flow* **8,** 217–226.

ROACHE, P. J. 1976 *Computational Fluid Dynamics.* Hermosa, Albuquerque, NM. ISBN 0-913478-05-09.

SELMER-OLSEN, S. 1991 Etude théorique et expérimentale des écoulements disphasiques en tuyère convergente divergente. Thèse de Doctorat, Inst. National Polytechnique de Grenoble, France.

SEVIK, M. & PARK, S. H. 1973 The splitting of drops and bubbles by turbulent fluid flow. *Trans. ASME, J. Fluids Engng* **95**, 53–60.

SUMMERFIELD, M., FOSTER, CH. R. & SWAN, W. C. 1954 Flow separation in an overexpanded supersonic exhaust nozzle. *J. Jet Propulsion* **24**, 319–321.

VROMMAN, T. 1988 Modélisation des écoulements critiques diphasiques dans un homogénéisateur de fluides pétroliers. Thèse de Docteur en Sciences Appliquées de l'Univ. Catholique de Louvain, Belgium.

WHITAM G. B. 1971 *Linear and Nonlinear Waves*, pp. 187–190. Wiley, New York.